Available online at www.sciencedirect.com
ScienceDirect
Journal of the European Ceramic Society 29 (2009) 439–450
www.elsevier.com/locate/jeurceramsoc

Citrate–nitrate auto-combustion synthesis of perovskite-type nanopowders: A systematic approach

F. Deganello [a,*], G. Marcì [b], G. Deganello [a,c]

[a] *Istituto per lo Studio dei Materiali Nanostrutturati, Consiglio Nazionale delle Ricerche, Via Ugo La Malfa 153, 90146 Palermo, Italy*
[b] *Dipartimento di Ingegneria Chimica dei Processi e dei Materiali, Università di Palermo, Viale delle Scienze, 90128 Palermo, Italy*
[c] *Dipartimento di Chimica Inorganica e Analitica "S. Cannizzaro", Università di Palermo, Viale delle Scienze, 90128 Palermo, Italy*

Received 7 April 2008; received in revised form 18 June 2008; accepted 19 June 2008
Available online 26 July 2008

Abstract

Citrate–nitrate auto-combustion synthesis is used to prepare an iron, a cobalt and a cerium-perovskite. The influence of different synthesis conditions on the combustion process, phase composition, textural and morphological properties is studied in detail by X-ray diffraction, nitrogen adsorption and scanning electron microscopy.

Results show that the combustion intensity increases from iron, to cerium, to cobalt-perovskite. Conversely, the combustion intensity decreases and thus the safety and the gain of the combustion process increase by using high fuel/oxidant ratios, low pH values or combustion reactors with high heat dispersion capacity.

High fuel/oxidant ratios increase particle size and may enhance dopant segregation. Low citric acid/metal nitrates ratios may cause precipitation of the most insoluble compounds or segregation of the dopant. High citric acid/metal nitrates ratios increase the formation temperature of the perovskite-type structure. Low pH values are deleterious for the phase composition and/or for the morphology of the final product, although at high pH values dopant segregation may occur.

Keywords: Citrate–nitrate auto-combustion synthesis; Powders-chemical preparation; Microstructure-final; Perovskites; Fuel cells

1. Introduction

Combustion synthesis is an easy and convenient method for the preparation of a variety of advanced ceramics, catalysts and nanomaterials.[1] In this technique, based on the principles of the propellant chemistry,[2] a thermally induced redox reaction takes place between an oxidant and a fuel. Many types of combustion synthesis exist which differ mainly in the physical state of the reactants or in the combustion modality.[1,3–7] By combustion-based methods it is possible to produce monophasic nanopowders with homogeneous microstructure, at lower temperatures or shorter reaction times, if compared with other conventional methods like solid-state synthesis[8,9] or nitrate method.[10,11] Citrate–nitrate auto-combustion synthesis (CNA) is a very popular solution combustion method,[12–14] where the fuel is citric acid and metal nitrates are used as metal and oxidant source. CNA method shows high similarities with the very well known Pechini process[15,16] and it can be more properly described as a "sol–gel combustion method".[17] Nevertheless the CNA method differs from Pechini process in that the nitrates are not previously eliminated as NOx, but remain in the mixture with metal citrates causing the auto-combustion.

The influence of the synthesis procedures on structure and electrical properties of solid oxide fuel cells (SOFCs) materials is becoming more and more important, especially when nanoceramics with superior quality are required.[5] Many essential aspects regarding combustion synthesis have been already quite exhaustively discussed in literature, like the effect of the type of organic fuel,[5,18–21] the influence of the fuel content,[5,6,12–14,22–24] the role of pH,[24–29] the effect of various combustion aids[30–32] and inert salts[33], the effect of a dry combustion[3] or a wet combustion[4] and the influence of the ignition modality[34] or of the ignition temperature.[35] Nevertheless, a deep understanding of the combustion-based methods has been hindered on one side by the tremendous number of variables and variants of the

* Corresponding author. Tel.: +39 091 6809387; fax: +39 091 6809399.
E-mail addresses: francesca.deganello@pa.ismn.cnr.it (F. Deganello), marci@dicpm.unipa.it (G. Marcì), g.deganello@pa.ismn.cnr.it (G. Deganello).

0955-2219/$ – see front matter © 2008 Elsevier Ltd. All rights reserved.
doi:10.1016/j.jeurceramsoc.2008.06.012

method, on the other side by the fact that very often too many parameters have been varied at the same time.[12–14,24]

The aim of this paper is to investigate some important questions about the CNA method, like the role of the fuel/oxidant ratio, of the citric acid/metal nitrates ratio and of the pH in the final mixed-oxide powder properties and the conditions of flame production. Moreover, the applicability of the CNA method for the synthesis of powders with different chemical composition is studied.

Three perovskite-type compounds with promising ion-conducting properties have been selected and prepared by CNA method. These are an iron-perovskite, $Sr_{0.85}Ce_{0.15}FeO_{3-x}$, a cobalt-perovskite, $La_{0.6}Sr_{0.4}Co_{0.95}Fe_{0.05}O_{3-x}$ and a cerium-perovskite, $BaCe_{0.9}Y_{0.1}O_{3-x}$. Ce-doped $SrFeO_3$ and Sr- and Fe-doped $LaCoO_3$ are known to possess important oxygen-conducting properties and have been already studied for application as solid oxide fuel cell cathodes.[36,37] Y-doped $BaCeO_3$ are hydrogen conducting compounds to be used as electrolytes in solid oxide fuel cells.[38–41] Different processing parameters have been used – maintaining the others strictly constant – and their effect on the structure, phase composition, morphology has been evaluated.

2. Experimental

2.1. Powder preparation

Stoichiometric amounts of highly purified metal nitrates were dissolved together in a minimum amount of distilled water to get a clear solution. An aqueous solution of citric acid was mixed with the nitrates solution. Citric acid has a double function, being the metal ion's complexant as well as the fuel. Citric acid/metal nitrates ratio (C/M) was varied between 1 and 4. Ammonium nitrate was added to regulate the fuel/oxidant ratio (F/O), represented by the citric acid/total nitrate ions ratio, which was varied between 0.4 and 1.6. Finally ammonia solution (30 wt.%) was slowly added to adjust the pH at the desired value, between 1 and 11.

In a 1-l beaker, immersed in an oil bath (high temperature silicon oil) in contact with a hot plate, the water solution was left to evaporate at 80 °C with continuous mechanical stirring, until a sticky gel was obtained. In order to carry out the gel decomposition under controlled conditions, the temperature of the oil bath was then raised gradually to 200 °C and finally the decomposed gel self-ignited. When temperatures higher than 200 °C were necessary to induce the auto-combustion, the beaker was put directly on the hotplate at 250–300 °C. The spontaneous combustion lasted for about 10–20 s and gave rise to the powdered product. Three different combustion reactors have been used for comparison (Pyrex glass, stainless steel and sintered alumina reactors). The combusted powders were then fired in static air at 1000 °C for 5 h, unless otherwise specified.

Three reference samples (one for each perovskite-type composition) were also prepared by using a conventional method based on the dissolution in water of metal nitrate precursors – without adding either citric acid or ammonia – followed by water evaporation at 80 °C under constant stirring and by thermal decomposition of nitrates in air at 350 °C ("nitrate method"). Since no filtration and/or separation steps were performed in the course of the synthesis process, the stoichiometry of the perovskite-type oxides was assumed to be the same as those of the weights of the metal nitrates before they were dissolved in water, unless oxide segregation occurred.

2.2. Powder characterization

X-ray diffraction (XRD) measurements were carried out on a SIEMENS D5000 X-ray powder diffractometer equipped with a Kristalloflex 760 X-ray generator and with a curved graphite monochromator which made possible the selection of the Cu Kα radiation (40 kV/30 mA). The 2θ step size was 0.03°. The integration time was 3 s per step, and the 2θ scan range was from 18° to 90°. The diffraction patterns have been analyzed by Rietveld refinement[42] using the GSAS package.[43] Chebyschev polynomials and Pearson VII functions have been chosen for the background and for the peak profile fitting, respectively. In the structure refinement lattice constants, Debye Waller factors, microstrain and full width half maximum (FWHM) have been considered as variables parameters. From fitting results, the structural parameters of the investigated compounds and, in particular, the cell edge lengths and the relative phase composition were obtained. An estimation of the crystal size values has been obtained from Scherrer equation in agreement with the GSAS package procedure. Agreement factors ("*R* values"[42]) below 10% have been obtained for all the structure refinements performed in this work. A standard deviation of ±0.003 Å for the refined cell parameters has been estimated in the experimental conditions used in this work. The obtained Debye Waller factors for the perovskite-type phases are in good agreement with the literature ones. Debye Waller factors of secondary phases have been set to the respective literature values.

Surface area of the powders (BET method[44]) and mesopore size distributions (BJH method[45]) have been determined by nitrogen adsorption/desorption measurements at 77 K, using a Sorptomatic 1900 Carlo Erba Instrument. All samples were pre-treated in vacuum at 250 °C for 1.5 h prior to the measurements.

The powder morphology has been observed by scanning electron microscopy (SEM). SEM images were obtained on samples upon which a thin layer of gold had been sputtered, using a model Philips XL30 ESEM microscope operating in high vacuum at 10 kV.

In the following discussion, $Sr_{0.85}Ce_{0.15}FeO_{3-x}$ will be referred as FE samples, $La_{0.6}Sr_{0.4}Co_{0.95}Fe_{0.05}O_{3-x}$ as CO samples and $BaCe_{0.9}Y_{0.1}O_{3-x}$ as CE samples.

3. Results and discussion

3.1. Effect of fuel/oxidant ratio

The maximum combustion intensity is observed at the stoichiometric F/O ratio for every chemical composition examined, in agreement with the results of Hwang and Wu[46] about the trend of the maximum combustion temperature with the F/O

ratio. Higher F/O ratios result in lower intensity of the auto-combustion reaction, as already observed by other authors,[47] whereas for much higher F/O values the auto-combustion becomes so slow that is hardly detectable. Nevertheless the range of explosive auto-combustion depends on the chemical composition and is different for FE, CE and CO samples: in a Pyrex glass beaker the flame combustion occurs until F/O = 0.3 for FE samples, until F/O = 0.4 for CE samples and until F/O = 0.5 for CO samples. The observed trend in the intensity of the auto-combustion process was then CO samples > CE samples > FE samples and it is in good agreement with the trend of stability constants (log β) of the cobalt (4.90), cerium (7.41) and iron–citrate (11.20) complexes.[48] High stability of the metal–citrate complex means more involvement of the ligand electrons in the chelation with the metal, which decreases the reducing power of the fuel. As a consequence, the auto-combustion reaction between the nitrate and the metal–citrate will be less intense. Since the combustion reaction is as a matter of facts a redox process,[2] the influence on the combustion process of the stability constant of metal citrates is more effective for metal ions with redox properties, like iron, cerium and cobalt, which are able to give electrons to the fuel, by changing their oxidation state. On the contrary we expect that poor effect will be shown by non-redox metal ions like strontium, barium and lanthanum, although they can form metal citrates as well and are present at high concentration in the mixture. Moreover, it is quite reasonable to make the hypothesis that the combustion process of compounds which are different but contain the same main redox element, will be the same. In order to better clarify this point further investigation is in progress, although first experiments seem quite encouraging.

It should be noted that even the gel characteristics are different for the three examined perovskite-type powders: before combustion the gel becomes a large swelling viscous mass for FE samples, whereas for CE and CO samples it is fully transformed into a dry black-brownish powder.

All the XRD patterns of FE, CE and CO powders calcined at 1000 °C/5 h contain only or mainly the desired perovskite-type phase. The structural data of the perovskite-type phases used for the Rietveld fits have been taken from the ICSD database. In particular, the $Sr_{0.85}Ce_{0.15}FeO_{3-x}$ phase (ICSD #249004), the $BaCe_{0.90}Y_{0.10}O_{3-x}$ phase (ICSD #72768) and the $La_{0.6}Sr_{0.4}CoO_{3-x}$ phase (ICSD #82817) have been used for the fit of FE, CE and CO samples, respectively. Nevertheless, under certain synthesis conditions some segregation occurs. For example high F/O ratios can favour CeO_2 segregation in FE samples (Fig. 1a) and $SrLaCoO_4$ segregation in CO samples (Fig. 1b). Correspondently, the a_0, b_0 and c_0 cell parameters of the perovskite-type main phase in CO samples increase abruptly from $a_0 = b_0 = c_0 = 5.411$ Å (angle = 60.3°) to $a_0 = b_0 = c_0 = 5.419$ Å (angle = 60.28°) when the F/O ratio changes from 0.7 to 0.8 and the perturbation of the perovskite-type phase caused by oxide segregation becomes substantial. Regarding FE samples, at low F/O ratios the perovskite-type phase shows a pure cubic structure with a cell parameter of $a_0 = b_0 = c_0 = 3.884$ Å. Nevertheless, by increasing the F/O ratio, the perovskite structure changes from cubic to a less symmetric

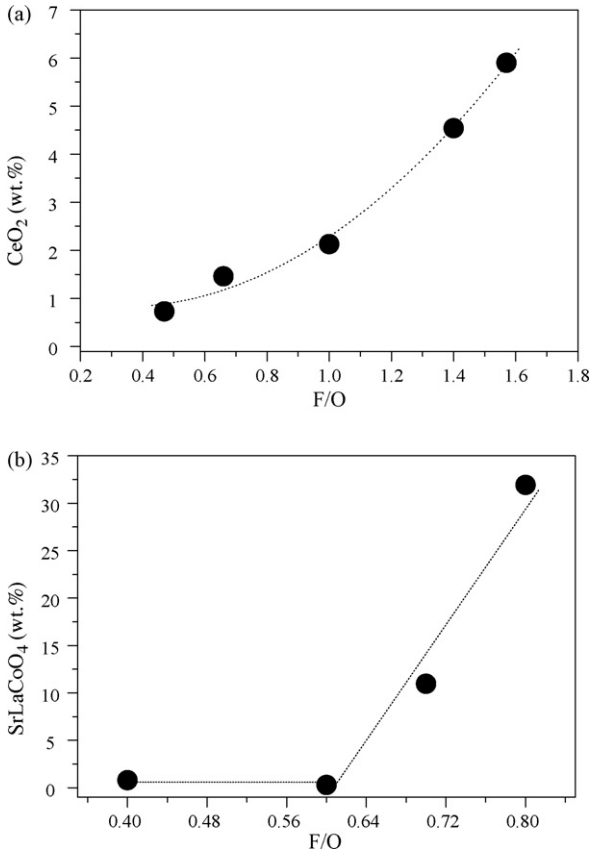

Fig. 1. wt.% of segregated CeO_2 in FE samples (C/M = 4, pH 9; calcined at 1000 °C/5 h) (a) and of segregated $SrLaCoO_4$ in CO samples (C/M = 2, pH 6; calcined at 1000 °C/5 h) (b) as a function of the fuel/oxidant ratio (F/O).

structure (Fig. 2), which unfortunately was not possible to identify properly. This change could be due to the strong perturbation of the perovskite structure caused by the CeO_2 segregation. This interpretation is further sustained by the fact that the same structural modification has been observed in FE samples at pH 1 where almost half of total cerium was present as segregated CeO_2 (see next paragraph).

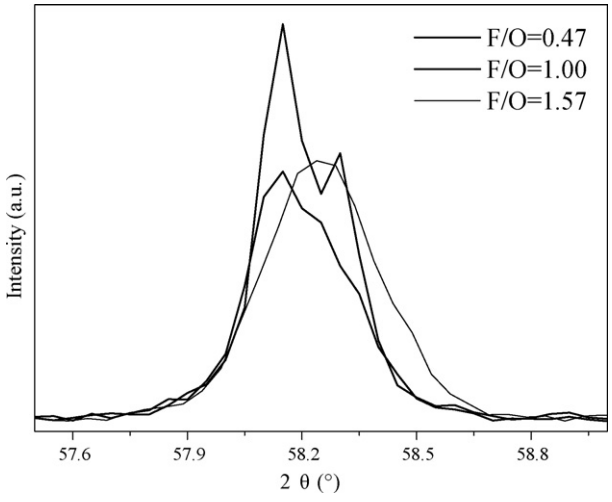

Fig. 2. Enlargement of the XRD patterns of FE samples (C/M = 4; pH 9) calcined at 1000 °C for 24 h and prepared by using different F/O ratios.

One possible explanation of the observed dopant segregation from the main perovskite-type phase is that, for high F/O ratios, the auto-combustion process becomes slower and let the atoms more time to rearrange in the segregated phase. To our knowledge, the effect of the fuel content on the phase composition of the calcined powders prepared by combustion-based methods has been evidenced only by few literature papers.[24,47,49–51] On the contrary, no segregation was observed for high F/O ratios in CE samples and the cell parameters of the orthorhombic perovskite-type main phase remain essentially constant to $a_0 = 8.774$, $b_0 = 6.244$ and $c_0 = 6.224$. Despite this, we cannot exclude that segregation may occur for F/O values higher than 0.8. It is plausible to argue that segregation at high F/O ratios may be favoured when the concentration of the dopant cation approaches the solubility limit in the perovskite. The solubility limit of cerium in $SrFeO_3$ is around 15 mol% and for higher dopant content cerium segregates as CeO_2[37]; the solubility limit of strontium in $LaCoO_3$ is ≤50 mol%, whereas for higher dopant content the rhombohedral Sr-doped $LaCoO_3$ transforms in the cubic La-doped $SrCoO_3$.[52] In this work, for CO samples, a Sr-rich phase like $SrLaCoO_4$ segregates (Fig. 1b) instead of the cubic La-doped $SrCoO_3$, whereas the rhombohedral perovskite remains still the main phase. Regarding the yttrium solubility limit in $BaCeO_3$, no clarity exists in the literature,[39–41] although for the samples studied in this work it has been estimated a solubility limit around 17 mol% after calcination at 1000 °C.[39]

Together with the already up cited segregated phase (CeO_2 for FE samples and $SrLaCoO_4$ for CO samples) minor amounts of other phases are detectable in the XRD pattern after thermal treatment at 1000 °C for 5 h. For example $SrCeO_3$ (ICSD #79003) and/or $SrFe_{12}O_{19}$ (ICSD #66403) were detected in FE samples and La_2O_3 (ICSD #26864) was detected in CO samples. Nevertheless after further thermal treatment at 1000 °C for 24 h, all the powders reach an equilibrium phase composition, the minor phases disappearing and the segregated phase decreasing slightly (Fig. 3).

All the calcined powders showed characteristic porous features due to the release of large amounts of gases during combustion, although FE samples (Fig. 4a and b) are more porous than CE (Fig. 4c and d) and CO samples (Fig. 4e and f). The mean primary particle size at low F/O ratios is around 200 nm for all the chemical composition examined, whereas high F/O ratios produce more coarse microstructure and larger particle size (Fig. 4) as already observed in the literature.[53,54] On the other hand crystal size remains constant at 120 nm for CE and CO samples. Regarding FE samples, at low F/O ratios crystal size is 120 nm as well, although it was not possible to obtain a crystal size trend with F/O since, by increasing F/O ratio, the perovskite structure changes from cubic to a less symmetric structure, which was not possible to identify properly, as already discussed in the previous paragraph. From the above results it is possible to calculate the mean agglomeration degree (particle size/crystal size) for CE and CO samples which is 1.5–2 crystals per particle at F/O = 0.4 for all the chemical compositions examined and increases slightly to 3–4 crystals per particle at F/O = 0.8. No agreement exists in the literature regarding the effect of the fuel content on the crystal size: some authors found an increase of crystal size with fuel content,[6,54] whereas other authors found the opposite trend.[55–57] Moreover, a volcano trend of the crystal size with fuel content is reported in literature,[53,58] although this trend could be interpreted as the overall result of the F/O and C/M variation.

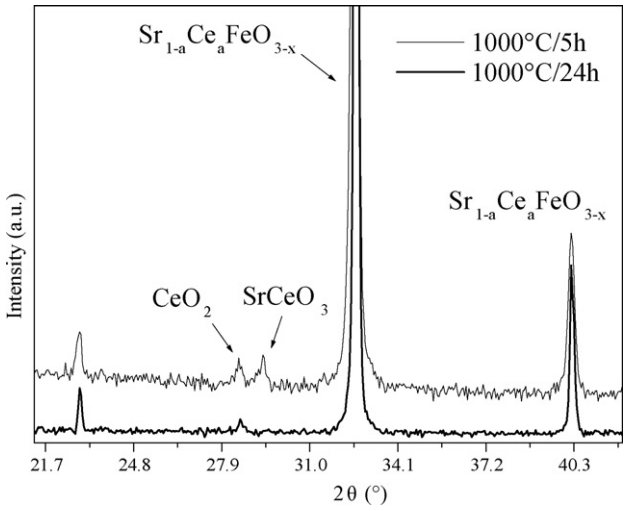

Fig. 3. Comparison between the XRD pattern of a FE sample (F/O = 0.47, C/M = 2, pH 9) calcined at 1000 °C for 5 h and the XRD pattern of the same sample calcined at 1000 °C for 24 h.

Adsorption–desorption isotherms and pore distributions are very similar for all the samples prepared by CNA method. Fig. 5a shows a typical adsorption–desorption isotherm. The isotherm can be classified as an isotherm of the type IV (IUPAC classification), which is characteristic of the mesoporous powders, as those investigated in this work. The hysteresis loop is of the type H_3 (IUPAC classification), suggesting that the majority of pores are slit-shaped with narrow entrances. Fig. 5b shows the narrow pore diameter distribution centered at 2 nm typical of the samples examined in this work. Surface area of all the samples examined in this work is mainly determined by the cumulative mesopore volume. In FE samples the surface area decreases with F/O until a minimum and then increases again for higher F/O values as shown in Fig. 6. This trend is probably the result of two different factors affecting the BET surface area: high F/O ratio means a less intense process and a slower combustion reaction, but high F/O ratio means as well large amount of gases coming from metal citrates decomposition, which enhances powder mesoporosity and surface area. Similar trends have been already found in literature.[5,46,54,59] Any slight difference can be ascribed to the fact that the authors of these cited references varied both the F/O and C/M ratios. For CE and CO samples the surface area is lower than 5 m^2/g and constant with F/O, although any trend in the BET area with F/O could have been masked by both the very short F/O range examined (0.4–0.8 instead of 0.4–1.6 used for FE samples) and the low surface area values measured at low F/O ratios. Other authors found that for CeO_2 powders prepared by CNA method the surface area decreases with F/O.[60] Neverthe-

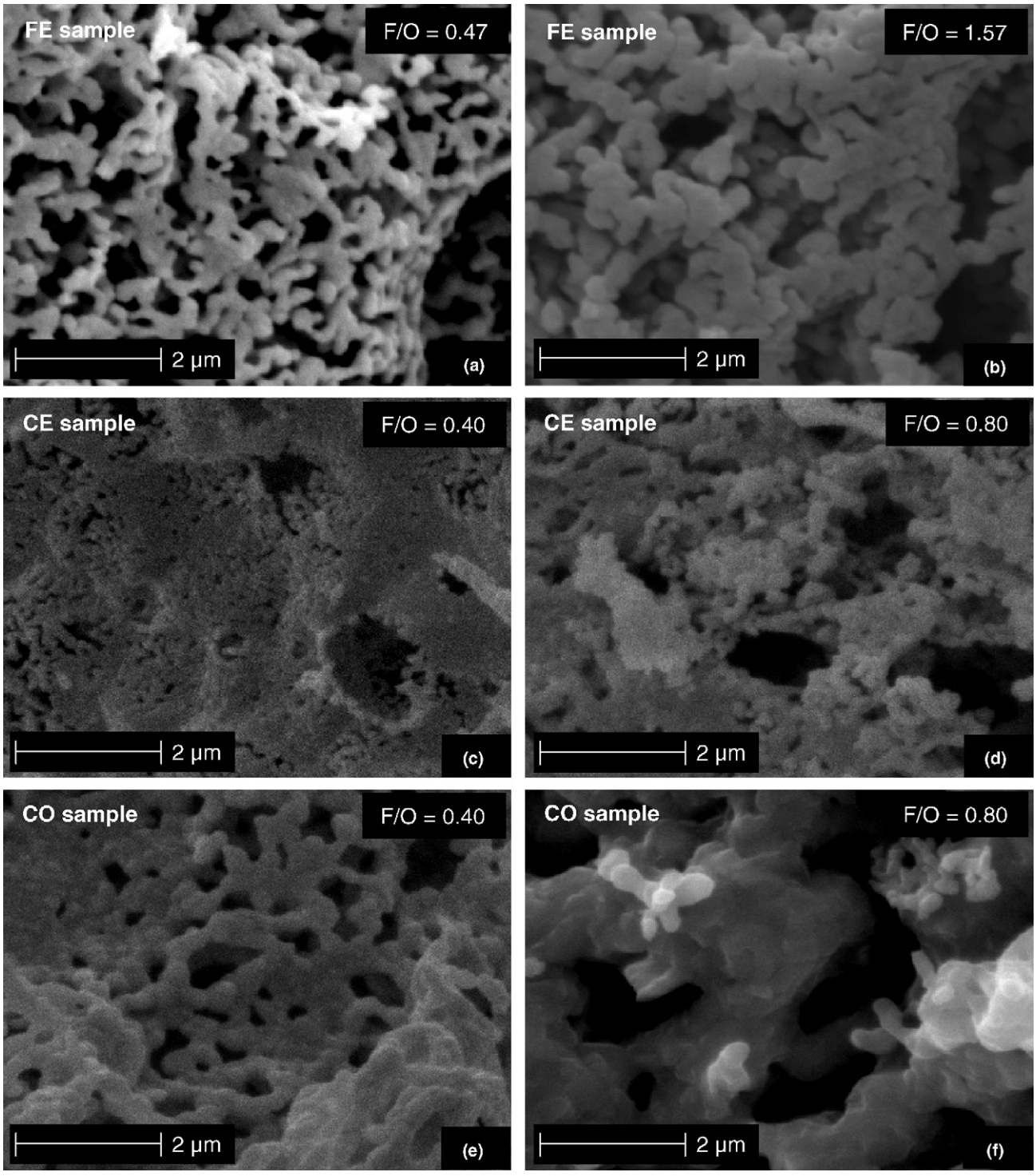

Fig. 4. SEM pictures of powdered (a and b) FE samples (C/M = 4; pH 9), (c and d) CE samples (C/M = 2; pH 6) and (e and f) CO samples (C/M = 2; pH 6) at low (a, c and e) and high (b, d and f) F/O ratios, calcined at 1000 °C for 5 h. The measured mean particle size is for FE samples: 209 nm (low F/O ratio) and 344 nm (high F/O ratios); for CE samples: 170 nm (low F/O ratio) and 270 nm (high F/O ratios); for CO samples: 232 nm (low F/O ratio) and 490 nm (high F/O ratios).

less, these authors managed to obtain higher surface area values because they considered the powders just after combustion.

A large surface area of the final powders could be quite important for FE and CO samples for application as cathodes, in order to increase the interaction with O_2 at the cathode interface or for CE samples in order to improve the sintering properties, when used as electrolyte materials.[7,61]

It has been reported that F/O may have some effect on the powders sinterability[34] and on the overall electrical properties of the electrolyte[56] and cathode materials,[47] although it is not clear

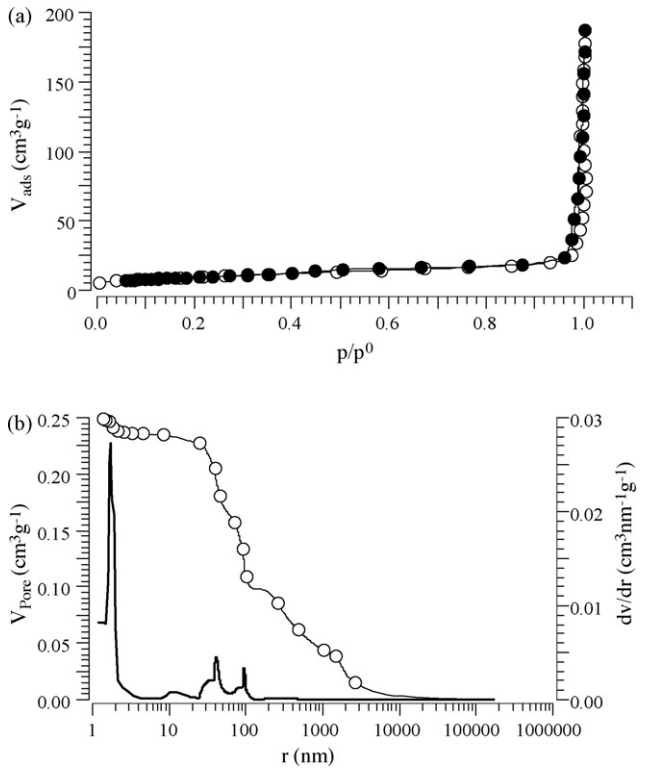

Fig. 5. (a) Nitrogen adsorption (open circles)–desorption (close circles) isotherm and (b) pore volume distribution (continuous line) and dV/dr (open circles) *vs.* pore radius for a FE sample (F/O = 0.47; C/M = 2; pH 9; calcined at 1000 °C/5 h).

if high F/O ratios improve[47] or reduce[56] the electrical properties of the materials.

3.2. Effect of pH

All the considerations made in the previous paragraph refers to powder prepared at pH 6 or 9. On the contrary at pH 1 the combustion process changes considerably: at 170 °C the gel transforms into a brownish powder, and the auto-combustion occurs when the temperature reaches a value higher than 250 °C. This behaviour is explained by the fact that at this low pH value the citric acid, being poorly dissociated, does not form any metal complex and decomposes at 175 °C. Similar results have been found in literature for cobalt ferrites.[27] As a consequence, no more citric acid is left for the citrate–nitrate auto-combustion reaction and perovskite decomposition as in the case of CE samples (Fig. 7a) or heavy segregation as for FE samples (Fig. 7b) may occur. It is worth to notice how the phase composition of the samples prepared by CNA method at pH 1 is very similar to the phase composition of the samples obtained by the nitrate method, where no citric acid is present, as shown in Fig. 8 for FE samples, where the amount of segregated CeO_2 is comparably high. While for CE samples pH 4 can be considered a good choice, since phase segregation does not occur if pH > pK_1 (3.15), for FE samples, in order to avoid or reduce the CeO_2 phase segregation, pH should be higher than pK_2 value of citric acid (4.77) as shown in Fig. 9a. The cell constant of the main perovskite-type phase in FE samples does not change for pH > pK_2, but the perovskite structure is perturbed for pH < pK_2, although no defined value for the cell parameter could be obtained, as already dis-

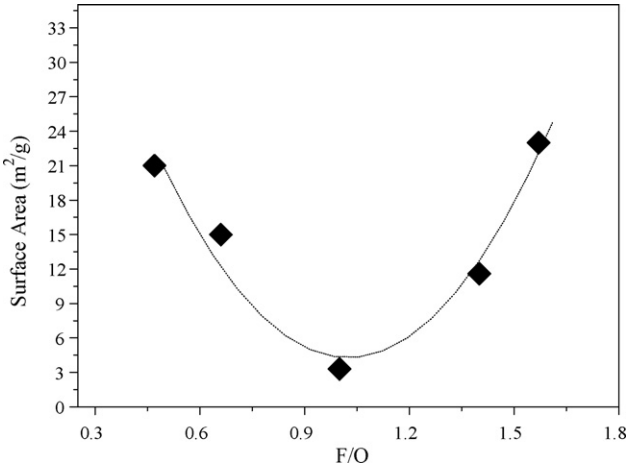

Fig. 6. Trend of the surface area (BET method) as a function of the F/O ratio for FE samples (C/M = 4; pH 9; calcined at 1000 °C/5 h).

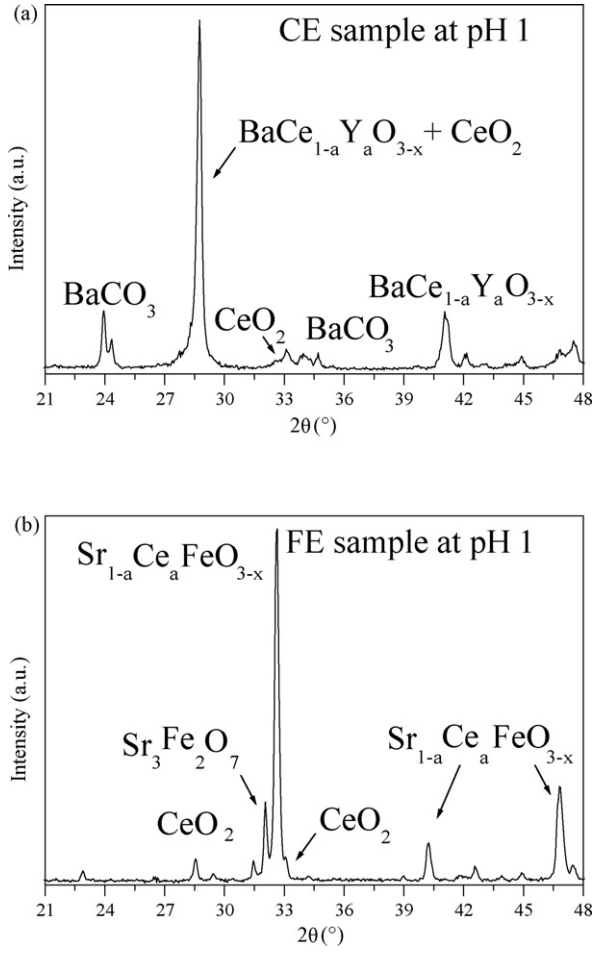

Fig. 7. XRD patterns of CE samples (F/O = 0.4; C/M = 2; calcined at 1000 °C/5 h) (a) and FE samples (F/O = 0.6; C/M = 1.5; calcined at 1000 °C/5 h) (b) prepared at pH 1.

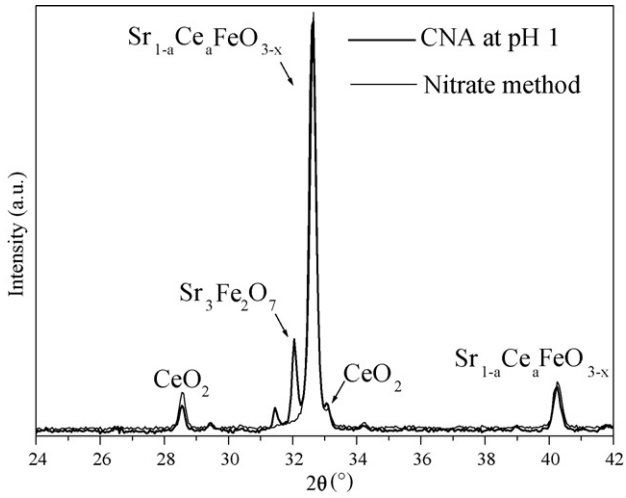

Fig. 8. Comparison between the XRD pattern of a FE sample prepared by CNA method (F/O = 0.6; C/M = 1.5) at pH 1 and the XRD pattern of a FE sample prepared by the nitrate method, both calcined at 1000 °C/5 h.

cussed in the previous paragraph. A very similar trend with pH has been found in literature for Sr- and Co-doped $LaFeO_3$.[25] These results are apparently in disagreement with the result of Majid et al.[9] who found that the best pH to obtain a pure $SrFeO_3$ is lower than 5. Nevertheless the authors did not add any dopant to the $SrFeO_3$, which could have segregated from the perovskite.

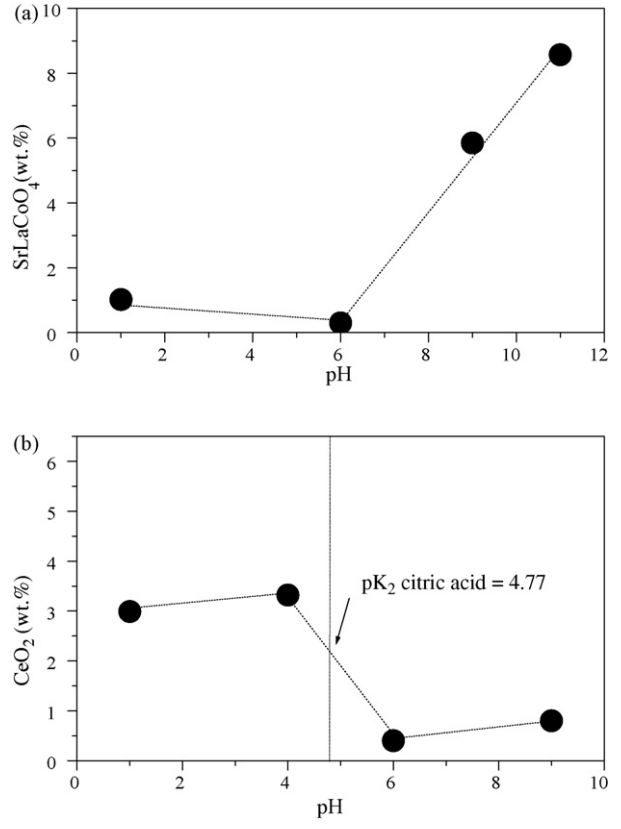

Fig. 9. Trend of the wt.% of the segregated phase as a function of pH for CO samples (F/O = 0.6; C/M = 2) (a) and FE samples (F/O = 0.6; C/M = 1.5) (b).

On the other side, high pH values can be deleterious for CO samples, where phase segregation occurs at pH higher than 6 (Fig. 9b). The cell constants of the main perovskite-type phase do not change with pH: higher percentage of dopant segregation is probably necessary in order to perturb the perovskite phase properly. A possible explanation for $SrLaCoO_4$ segregation at high pH could be that some more stable mixed strontium–cobalt–lanthanum citrates form or that ammonia perturbs the metal citrates gel network, favouring $SrLaCoO_4$ segregation. This result is in apparent contradiction with the results of Xu et al.[8] where a similar composition prepared by a very similar synthesis method shows phase segregation at low pH, but not at high pH. Nevertheless it is possible that, at the calcination temperature of 750 °C used by Xu et al.[8] not all the phases are well crystallized and it is not possible to completely exclude $SrLaCoO_4$ and Co_3O_4 segregation at pH 9. Moreover, Xu et al.[8] used a F/O = 0.5, which is slightly lower than the F/O ratio used in this work and for CO samples substantial segregation occurs for F/O ratios higher than 0.6, as we have demonstrated in Section 3.1.

Low pH values have a negative effect on the final powder morphology as well (Fig. 10). The powders prepared at pH 1 (partial complexation of metal cations) have irregular texture and larger particles size for every chemical composition examined. Fig. 10 shows the progressive positive effect of citric acid complexation on the final powder morphology, from the nitrate method (no citric acid), through the CNA method at pH 1, to the CNA method at pH 6 (full complexation of metal cations). As a general consideration it is possible to observe that the particles size values of the samples prepared by CNA method at pH 1 are more similar to those of the samples obtained by the nitrate method, although in the first case particle shape and particle size have a more regular distribution. On the other side, the particle shapes of the samples prepared by CNA method at pH 1 and 6 are quite similar to each other, although the particles size of the last one are, generally, smaller (Fig. 10). From these results it can be concluded that the optimum pH seems to be dependent both on the metal complexing strength and on the presence of metal compounds with poor solubility, although pH 5–6 can be optimum pH for many cases.

By increasing pH, the combustion process becomes more intense as already observed by other authors.[26] In particular, for CE samples no flame appears for pH 6 (F/O = 0.4; C/M = 2; Pyrex glass beaker), but at pH 9 high flame is produced during the auto-combustion. The reason why pH can influence the combustion process, even after water evaporation and gel decomposition until 200 °C, is that some ammonia probably remains in the gel structure until auto-combustion, as observed by other authors.[17]

3.3. Effect of citric acid/metal nitrates ratio

The optimal C/M value highly depends on the chemical composition of the combustion mixture and in particular on the interaction of citric acid with metal cations and on the formation of insoluble metal compounds. As a consequence it is difficult to find out some general rules.

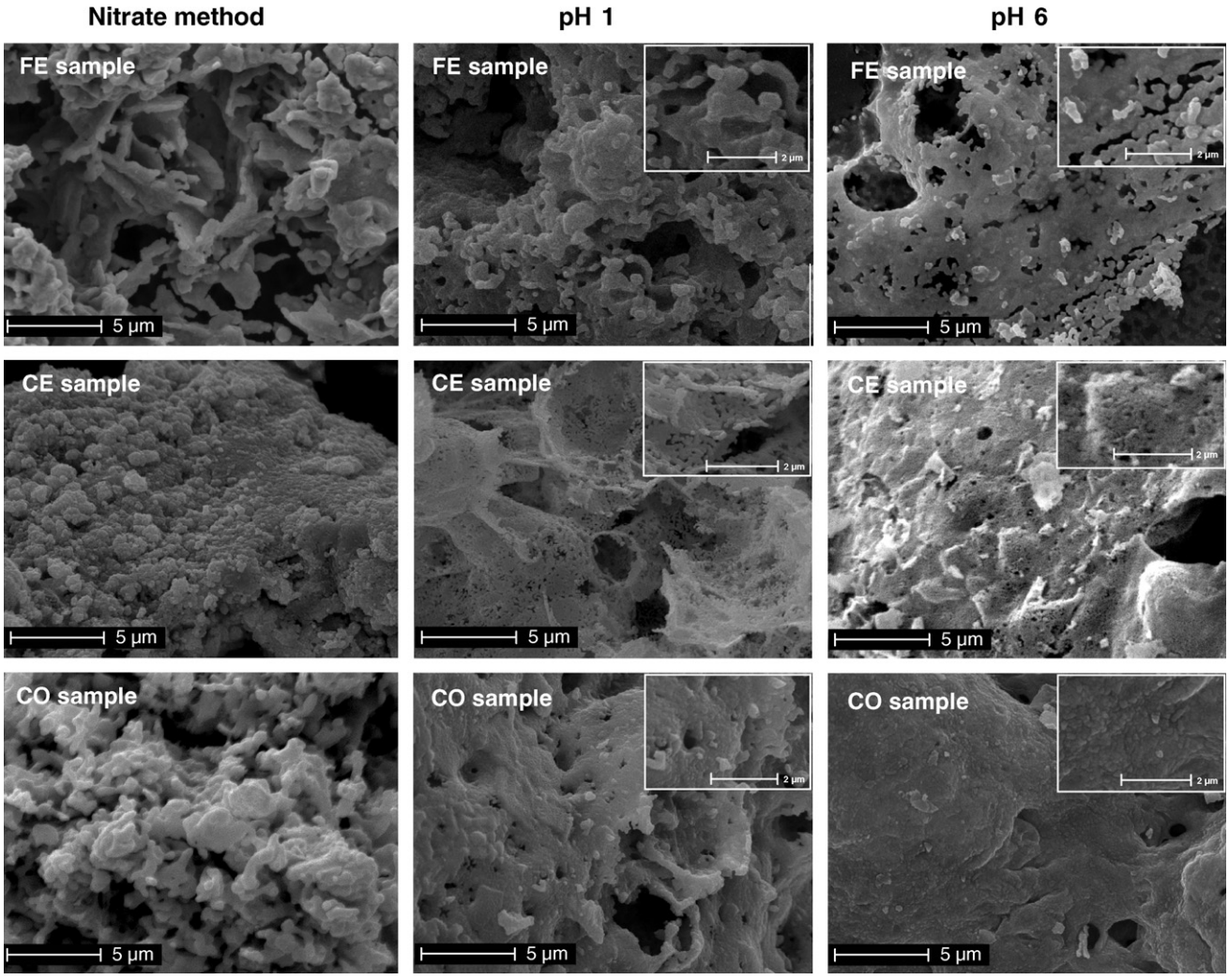

Fig. 10. SEM pictures of powdered FE samples (F/O = 0.6; C/M = 1.5), CE samples (F/O = 0.4; C/M = 2) and CO samples (F/O = 0.6; C/M = 2) (from the top to the bottom), at pH 1 (middle column) and pH 6 (right column) in comparison with the samples prepared by the nitrate method (left column), after calcination at 1000 °C for 5 h.

C/M ratio may have some effect on the morphology of the powders calcined at 1000 °C, without affecting their phase composition, like for FE and CE samples. In these cases, the cell constants do not change with C/M. For example, in FE samples a very low surface area was measured at C/M = 1.2, which increased for C/M = 2 and decreased slightly again for higher C/M values (Table 1). Although the interpretation of this trend is still not clear, it is in agreement with the correspondent trend of the agglomeration degree with C/M (Table 1), according to the fact that for higher agglomeration degrees lower surface areas are obtained.[33]

Another example of the effect of C/M ratio on the morphology is the large particle size (540 nm) and non-homogeneous texture observed for CE powders prepared at C/M = 1, which is probably caused by the $BaCO_3$ precipitation occurred before the gel formation.

In general, low C/M ratios mean low cost and low organics to burn out, although, from the examples described above, high C/M values seem more pertaining. Nevertheless in some cases high C/M ratios may affect the phase composition of the final powders, as for CO samples, where some phase segregation (2.7 wt.% of $SrLaCoO_4$) occurred for C/M = 4. A possible explanation of this result can be related on one side with the dependence of the phase segregation with pH described for CO samples in Section 3.2; on the other side it can be related with the slight increase of the ammonia concentration for high C/M

Table 1
Morphological properties of FE samples for different C/M ratios

C/M	Particle size (nm)	Crystal size (nm)	Agglomeration degree (particle size/crystal size)	Surface area (m^2/g)
1.2	234	69	3.4	5
2	200	116	1.7	33
4	209	91	2.3	21

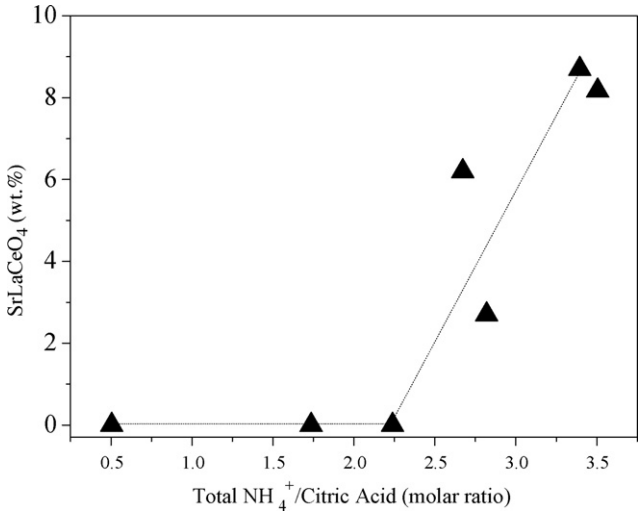

Fig. 11. Trend of segregated $SrLaCoO_4$ as a function of the Total NH_4^+/citric acid ratio in CO samples prepared at F/O = 0.6, but at different pH and C/M values.

ratios: in order to investigate the effect of C/M ratio on the final powder, pH and F/O values were maintained strictly constant and NH_4NO_3 was introduced as F/O regulator. It has been argued that segregation in CO samples depends more on the total NH_4^+/citric acid ratio than on the pH itself, as clearly shown in Fig. 11, where for a total NH_4^+/citric acid ratio >2 segregation in CO samples increases substantially. The cell constant of the perovskite-type main phase in CO samples does not change with C/M, because the entity of the segregation is too low, as already discussed in the previous paragraph.

The C/M ratio has an important effect on the formation temperature of perovskite-type structure as shown in Fig. 12a for FE samples: for C/M = 2 almost 100 wt.% perovskite is present after calcination at 600 °C for 5 h, whereas, at higher C/M values, the diffraction peak of the perovskite-type structure almost disappears and longer calcinations times at the same temperature or higher temperatures are necessary in order to obtain the perovskite-type structure. A possible explanation of this result could be that the excess of not-bounded citric acid produces residual organic materials which at 600 °C transform into isolate carbonates and oxides, instead of forming the multicomponent perovskite. A similar interpretation has been proposed by other authors.[62] Conversely, the XRD patterns of two samples with different F/O values (and the same C/M value) are identical regarding the phase composition after calcinations at 600 °C for 5 h as demonstrated for FE samples in Fig. 12b.

Nevertheless the perovskite-type structure formation temperature depends as well on the chemical composition considered: FE and CO powders calcined at 600 °C contain mainly the perovskite-type phase, whereas CE powders calcined at the same temperature contain just $BaCO_3$ and CeO_2, which convert to a substantial fraction of perovskite only after calcination at 800 °C (Fig. 13). The XRD pattern of the powders just after combustion is different for different chemical composition. If a stoichiometric F/O value is used, the perovskite structure is directly obtained after combustion, as shown for FE samples in Fig. 12c. For

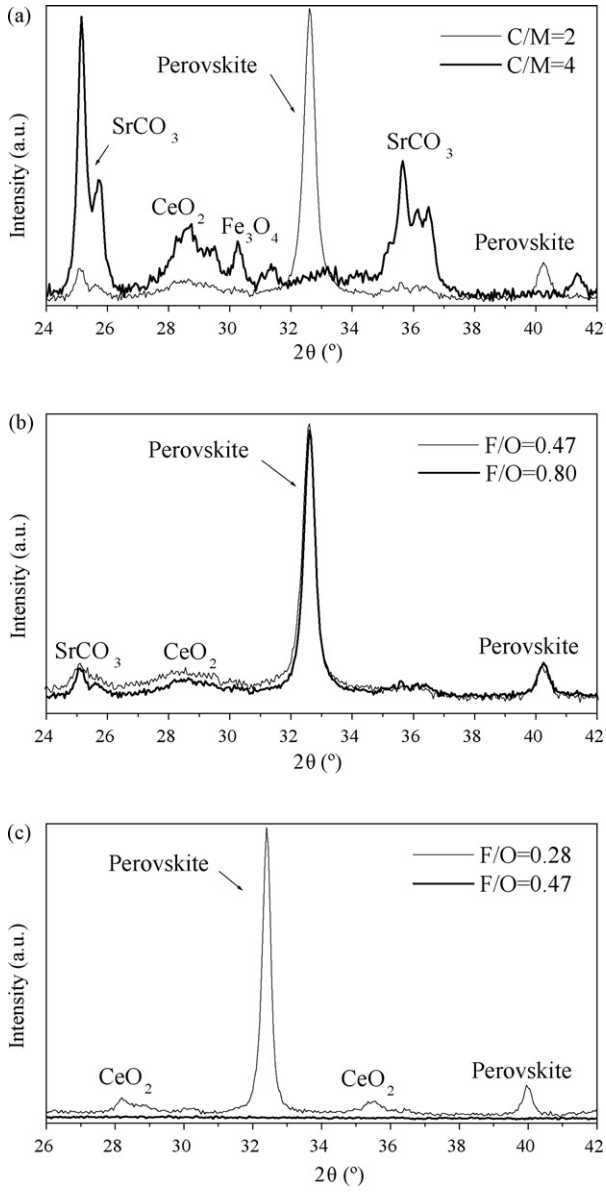

Fig. 12. XRD patterns of FE samples calcined at 600 °C for 5 h and prepared by using different C/M ratios (F/O = 0.47; pH 9) (a) or different F/O ratios (C/M = 2; pH 9) (b); XRD patterns of FE samples just after combustion prepared by using a stoichiometric or an over-stoichiometric F/O ratio (C/M = 2; pH 9) (c).

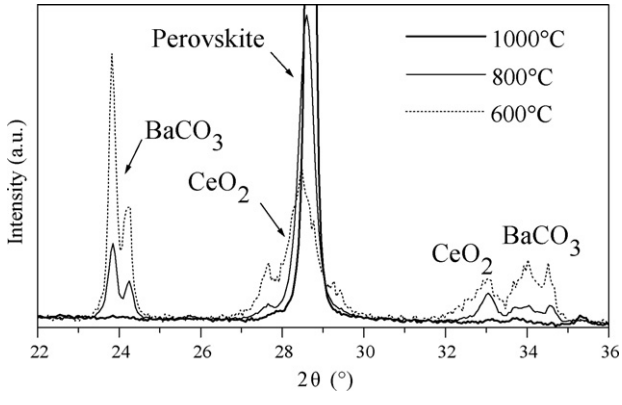

Fig. 13. XRD patterns of CE samples prepared by using C/M = 2 (F/O = 0.4, pH 9) and calcined at 600 °C, 800 °C and 1000 °C.

higher F/O ratios the combusted powder is totally amorphous in FE samples (Fig. 12c), but shows poorly crystallized diffraction peaks in CE (only $BaCO_3$ and CeO_2) and CO samples (the perovskite-type structure is already visible), in agreement with the different intensity of the process for these three chemical compositions examined (see Section 3.1).

A lower formation temperature of the perovskite-type structure may be of special importance for FE and CO samples, if they have to be deposited at low temperature on a dense electrolyte surface in order to obtain a porous cathode.[36,63] The results above discussed indicate that in most cases a C/M value of 2 can be considered a good choice of compromise. Too low C/M ratios may have some influence on the morphology, but too high C/M ratios may negatively affect the phase composition of the powders and the perovskite-type formation temperature.

3.4. Identification of the safety conditions

The auto-combustion reaction can be explosive, yielding a high flame which quickly propagates through the reactant mixture. Therefore, safety becomes more and more important when many grams of powder have to be prepared by auto-combustion synthesis, as observed by other authors.[5] Moreover, if the combustion reaction is more explosive, more powder is displaced from the combustion beaker and the product is thus lost. Even if the combustion reaction takes place very calmly, without flame production, only 80% of the product can be recovered at low F/O ratios, because some of the very fluffy powder flies away with the combustion gases. At F/O = 0.8, where the intensity of the process is decreased, a 90% of recovery can be attained. For these reasons, in this work, special care has been taken in the identification of the safety conditions. In Section 3.1 it is described that the combustion intensity decreases with F/O ratio and changes with the phase composition of the chemical mixture. Moreover, the combustion intensity increases with pH value as shown in Section 3.2. Another important point is the material of the combustion beaker. On this respect, by comparing three combustion reactors made of different materials (sintered alumina, Pyrex glass and stainless steel) and by fixing all the other parameters, results show that sintered alumina reactor displays the highest combustion intensity, whereas stainless steel reactor displays the lowest one. This trend has been associated with the different dispersion capacity of the three materials. In summary, when this is possible, higher F/O ratios, lower pH values and combustion reactors with higher heat dispersion capacity are recommended in order to conduct safely the combustion synthesis.

4. Conclusion

This work gives some general guidelines in order to obtain multicomponent nanopowders with desired properties by using citrate–nitrate auto-combustion synthesis in a smouldering combustion modality. The systematic investigation of the relationship between synthesis and properties of the final powder has been made possible by varying every processing parameter one by one.

The fuel/oxidant ratio has clearly the most intense influence on the structural and morphological properties of the powders. Low fuel/oxidant ratios are recommended in some cases in order to avoid segregation of the dopant and to obtain powders with small particle size. Nevertheless, high fuel/oxidant ratios may be considered a better choice, in order to avoid dangerous flame production and massive powder volatilization. Low pH and the use of stainless steel beakers are two other recommended conditions which decrease the explosivity of the combustion reaction.

Low pH are generally deleterious for the phase composition and/or for the morphology of the final product and high pH values may cause dopant segregation.

The citric acid/metal nitrates should be carefully selected in order to avoid precipitation of the most insoluble compounds or segregation of the dopant. Moreover, high C/M values increase the formation temperature of the perovskite-type structure.

The systematic investigation performed in this work has allowed the identification, for the three chemical compositions examined, of a general response to the variation of the various processing parameters, although in some cases a different behaviour has been shown by the three perovskite-type compounds. These differences have been ascribed on one side to the specific chemistry of the mixture and on the other side to the different metal citrate stability constants of the main redox cations present in the perovskite and pointed out to the necessity of an accurate selection of the processing parameters.

Acknowledgements

The authors are thankful to Dr. Francesco Giordano for his support in the XRD measurements and to Prof. E. Traversa for useful discussion. Moreover, the financial support of FISR – “Celle a combustibile ad elettroliti polimerici e ceramici: dimostrazione di sistemi e sviluppo di nuovi materiali” and PRIN-MUR (2006094904_002) – “Ceramici protonici per celle a combustibile” is greatly acknowledged.

References

1. Patil, K. C., Aruna, S. T. and Mimani, T., Combustion synthesis: an update. *Curr. Opin. Solid State Mater. Sci.*, 2002, **6**, 507–512.
2. Jain, S. R., Adiga, K. C. and Pai Verneker, V. R., A new approach to thermochemical calculations of condensed fuel–oxidizer mixtures. *Combust. Flame*, 1981, **40**, 71–79.
3. Hwang, C.-C., Huang, T.-H., Tsai, J.-S., Lin, C.-S. and Peng, C.-H., Combustion synthesis of nanocrystalline ceria (CeO_2) powders by a dry route. *Mater. Sci. Eng. B*, 2006, **132**, 229–238.
4. Mukasyan, A. S., Epstein, P. and Dinka, P., Solution combustion synthesis of nanomaterials. *Proc. Combust. Inst.*, 2007, **31**, 1789–1795.
5. Tyagi, A. K., Chavan, S. V. and Purohit, R. D., A visit to the fascinating world of nano-ceramics powders via solution-combustion. *Ind. J. Pure Appl. Phys.*, 2006, **44**, 113–118.
6. Chen, W., Li, F. and Yu, J., A facile and novel route to high surface area ceria-based nanopowders by salt-assisted solution combustion synthesis. *Mater. Lett.*, 2006, **60**, 57–62.
7. Bedekar, V., Grover, V., Nair, S., Purohit, R. D. and Tyagi, A. K., Nanocrystalline electroceramics by combustion method. *Synth. React. Inorg. Met.-Org. Nano-Met. Chem.*, 2007, **37**, 321–326.
8. Xu, Q., Huang, D.-P., Chen, W., Lee, J.-H., Wang, H. and Yuan, R.-Z., Citrate method synthesis, characterization and mixed electronic–ionic conduction

properties of $La_{0.6}Sr_{0.4}Fe_{0.2}Co_{0.8}O_3$ perovskite-type complex oxides. *Scr. Mater.*, 2004, **50**, 165–170.
9. Majid, A., Tunney, J., Argue, S., Wang, D., Post, M. and Margeson, J., Preparation of $SrFeO_{2.85}$ perovskite using a citric acid assisted Pechini-type method. *J. Alloys Compd.*, 2005, **398**, 48–54.
10. Palmisano, P., Russo, N., Fino, P., Fino, D. and Badini, C., High catalytic activity of SCS-synthesized ceria towards diesel soot combustion. *Appl. Catal. B: Environ.*, 2006, **69**, 85–92.
11. Carvalho, M. D., Costa, F. M. A., da Silva Pereira, I., Wattiaux, A., Bassat, J. M., Grenier, J. C. *et al.*, New preparation method of $La_{n+1}Ni_nO_{3n+1-\delta}$ ($n = 2$, 3). *J. Mater. Chem.*, 1997, **7**, 2107–2111.
12. Marinsek, M., Zupan, K. and Maèek, J., Ni-YSZ cermet anodes prepared by citrate/nitrate combustion synthesis. *J. Power Sources*, 2002, **106**, 178–188.
13. Chakroborty, A., Das Sharma, A., Maiti, B. and Maiti, H. S., Preparation of low-temperature sinterable $BaCe_{0.8}Sm_{0.2}O_3$ powder by autoignition technique. *Mater. Lett.*, 2002, **57**, 862–867.
14. Mali, A. and Ataie, A., Influence of the metal nitrates to citric acid molar ratio on the combustion process and phase constitution of barium hexaferrite particles prepared by sol–gel combustion method. *Ceram. Int.*, 2004, **30**, 1979–1983.
15. Hernandez, T. and Bautista, M. C., The role of the synthesis route to obtain densified TiO_2-doped alumina ceramics. *J. Eur. Ceram. Soc.*, 2005, **25**, 663–672.
16. Pechini, M., US Patent, 3,330,697; 1967.
17. Epifani, M., Melissano, E., Pace, G. and Schioppa, M., Precursors for the combustion synthesis of metal oxides from the sol–gel processing of metal complexes. *J. Eur. Ceram. Soc.*, 2007, **27**, 115–123.
18. Erri, P., Pranda, P. and Varma, A., Oxidizer–fuel interactions in aqueous combustion synthesis. 1. Iron(III) nitrate-model fuels. *Ind. Eng. Chem. Res.*, 2004, **43**, 3092–3096.
19. Hwang, C.-C., Wu, T.-Y., Wan, J. and Tsai, J. S., Development of a novel combustion synthesis method for synthesizing of ceramic oxide powders. *Mater. Sci. Eng. B*, 2004, **111**, 49–56.
20. Li, F., Hu, K., Li, J., Zhang, D. and Chen, G., Combustion synthesis of γ-lithium aluminate by using various fuels. *J. Nucl. Mater.*, 2002, **300**, 82–88.
21. Wu, K. H., Ting, T. H., Yang, C. C. and Wang, G. P., Effect of complexant/fuel on the chemical and electromagnetic properties of SiO_2-doped Ni–Zn ferrite. *Mater. Sci. Eng. B*, 2005, **123**, 227–233.
22. Mukasyan, A. S., Costello, C., Sherlok, K. P., Lafarga, D. and Varma, A., Perovskite membranes by aqueous combustion synthesis: synthesis and properties. *Sep. Purif. Technol.*, 2001, **25**, 117–126.
23. Hosseini Vajargah, S., Madaah Hosseini, H. R. and Nemati, Z. A., Preparation and characterization of yttrium iron garnet (YIG) nanocrystalline powders by auto-combustion of nitrate–citrate gel. *J. Alloys Compd.*, 2007, **430**, 339–343.
24. Hwang, B. J., Santhanam, R. and Liu, D. G., Effect of various synthetic parameters on purity of $LiMn_2O_4$ spinel synthesized by a sol–gel method at low temperature. *J. Power Sources*, 2001, **101**, 86–89.
25. Wu, Z., Zhou, W., Jin, W. and Xu, N., Effect of pH on synthesis and properties of perovskite oxide via a citrate process. *AlChE J.*, 2006, **52**, 769–776.
26. Yue, Z., Guo, W., Zhou, J. and Li, L., Synthesis of nanocrystalline ferrites by sol–gel combustion process: the influence of pH value of solution. *J. Magn. Magn. Mater.*, 2004, **270**, 216–223.
27. Cannas, C., Falqui, A., Musinu, A., Peddis, D. and Piccaluga, G., $CoFe_2O_4$ nanocrystalline powders prepared by citrate–gel methods: synthesis, structure and magnetic properties. *J. Nanopartic. Res.*, 2006, **8**, 255–267.
28. Xu, G., Ma, H., Zhong, M., Zhou, J., Yue, Y. and He, Z., Influence of pH on characteristics of $BaFe_{12}O_{19}$ powder prepared by sol–gel auto-combustion. *J. Magn. Magn. Mater.*, 2006, **301**, 383–388.
29. Peng, T., Liu, X., Dai, K., Xiao, J. and Song, H., Effect of acidity on the glycine–nitrate combustion synthesis of nanocrystalline alumina powder. *Mater. Res. Bull.*, 2006, **41**, 1638–1645.
30. Civera, A., Pavese, M., Saracco, G. and Specchia, V., Combustion synthesis of perovskite-type catalysts for natural gas combustion. *Catal. Today*, 2003, **83**, 199–211.
31. Burgos-Montes, O., Moreno, R., Colomer, M. T. and Fariñas, J. C., Influence of combustion aids on suspension combustion synthesis of mullite powders. *J. Eur. Ceram. Soc.*, 2006, **26**, 3365–3372.
32. Biamino, S. and Badini, C., Combustion synthesis of lanthanum chromite starting from water solutions: investigation of process mechanism by DTA-TGA-MS. *J. Eur. Ceram. Soc.*, 2004, **24**, 3021–3024.
33. Chen, W., Li, F., Yu, J. and Liu, L., A facile and novel route to high surface area ceria-based nanopowders by salt-assisted solution combustion synthesis. *Mater. Sci. Eng. B*, 2006, **133**, 151–156.
34. Chandramouli, V., Anthonysamy, S. and Vasudeva Rao, P. R., Combustion synthesis of thoria—a feasibility study. *J. Nucl. Mater*, 1999, **265**, 255–261.
35. Poth, J., Haberkorn, R. and Beck, H. P., Combustion-synthesis of $SrTiO_3$. Part I. Synthesis and properties of the ignition products. *J. Eur. Ceram. Soc.*, 2000, **20**, 707–713.
36. Deganello, F., Esposito, V., Miyayama, M. and Traversa, E., Cathode performance of nanostructured $La_{1-a}Sr_aCo_{1-b}Fe_bO_{3-x}$ on a $Ce_{0.8}Sm_{0.2}O_2$ electrolyte prepared by citrate–nitrate autocombustion. *J. Electrochem. Soc.*, 2007, **154**, A89–A96.
37. Deganello, F., Liotta, L. F., Longo, A., Casaletto, M. P. and Scopelliti, M., Cerium effect on the phase structure, phase stability and redox properties of Ce-doped strontium ferrates. *J. Solid State Chem.*, 2006, **179**, 3406–3419.
38. Longo, A., Giannici, F., Balerna, A., Ingrao, C., Deganello, F. and Martorana, A., Local environment of yttrium in Y-doped barium cerate compounds. *Chem. Mater.*, 2006, **18**, 5782–5788.
39. Giannici, F., Longo, A., Deganello, F., Balerna, A., Arico', A. S. and Martorana, A., Local environment of barium, cerium and yttrium in $BaCe_{1-x}Y_xO_{3-\delta}$ ceramic protonic conductors. *Solid State Ionics*, 2007, **178**, 587–591.
40. Takeuchi, K., Loong, C.-K., Richardson, J. W., Guan Jr., J., Dorris, S. E. and Balachandran, U., The crystal structures and phase transitions in Y-doped $BaCeO_3$: their dependence on Y concentration and hydrogen doping. *Solid State Ionics*, 2000, **138**, 63–77.
41. Suksamai, W. and Metcalfe, I. S., Measurement of proton and oxide ion fluxes in a working Y-doped $BaCeO_3$ SOFC. *Solid State Ionics*, 2007, **178**, 627–634.
42. McCusker, L. B., Von Dreele, R. B., Coxd, D. E., Louer, D. and Scardi, P., Rietveld refinement guidelines. *J. Appl. Cryst.*, 1999, **32**, 36–50.
43. Larson, A. C. and Von Dreele, R. B., *GSAS General Structure Analysis System, LANSCE, MS-H 805*. Los Alamos National Laboratory, Los Alamos, NM 87545, USA, 1998.
44. Brunauer, S., Emmett, P. H. and Teller, E., Adsorption of gases in multimolecular layers. *J. Am. Chem. Soc.*, 1938, **60**, 309–319.
45. Barret, E. P., Joyner, L. G. and Halenda, P. P., The determination of pore volume and area distributions in porous substances. I. Computations from nitrogen isotherms. *J. Am. Chem. Soc.*, 1951, **73**, 373–380.
46. Hwang, C.-C. and Wu, T.-Y., Synthesis and characterization of nanocrystalline ZnO powders by a novel combustion synthesis method. *Mater. Sci. Eng. B*, 2004, **111**, 197–206.
47. Guo, R. S., Wei, Q. T., Li, H. L. and Wang, F. H., Synthesis and properties of $La_{0.7}Sr_{0.3}MnO_3$ cathode by gel combustion. *Mater. Lett.*, 2006, **60**, 261–265.
48. Smith, R. M. and Martell, A. E., *Critical Stability Constants*, *2*. Plenum Press, New York, 1975.
49. Chick, L. A., Maupin, G. D. and Pederson, L. R., Glycine–nitrate synthesis of a ceramic–metal composite. *Nanostruct. Mater.*, 1994, **4**, 603–615.
50. Bhaduri, S., Zhou, E. and Bhaduri, S. B., Auto ignition processing of nanocrystalline α-Al_2O_3. *Nanostruct. Mater.*, 1996, **7**, 487–496.
51. Jung, C.-H., Jalota, S. and Bhaduri, S. B., Quantitative effects of fuel on the synthesis of Ni/NiO particles using a microwave-induced solution combustion synthesis in air atmosphere. *Mater. Lett.*, 2005, **59**, 2426–2432.
52. Petrov, A. N., Kononchuk, O. F., Andreev, A. V., Cherepanov, V. A. and Kofstad, P., *Solid State Ionics*, 1995, **80**, 189–199.
53. Singh, K. A., Pathak, L. C. and Roy, S. K., Effect of citric acid on the synthesis of nano-crystalline yttria stabilized zirconia powders by nitrate–citrate process. *Ceram. Int.*, 2007, **33**, 1463–1468.
54. Li, J., Pan, Y., Qiu, F., Wu, Y. and Guo, J., Nanostructured Nd:YAG powders via gel combustion: the influence of citrate-to-nitrate ratio. *Ceram. Int.*, 2008, **34**, 141–149.
55. Azadmanjiri, J. and Seyyed Ebrahimi, S. A., The effects of pH and citric acid concentration on the characteristics of nanocrystalline $NiFe_2O_4$ powder

synthesized by a sol–gel autocombustion method. *Phys. Met. Metallogr.*, 2006, **102**, S21–S23.
56. Xu, H., Yan, H. and Chen, Z., Sintering and electrical properties of $Ce_{0.8}Y_{0.2}O_{1.9}$ powders prepared by citric acid–nitrate low-temperature combustion process. *J. Power Sources*, 2006, **163**, 409–414.
57. Zhang, J. and Gao, L., Antimony-doped tin oxide nanocrystallites prepared by a combustion process. *Mater. Lett.*, 2004, **58**, 2730–2734.
58. Lian, J. S., Zhang, X. Y., Zhang, H. P., Jiang, Z. H. and Zhang, J., Synthesis of nanocrystalline NiO/doped CeO_2 compound powders through combustion of citrate/nitrate gel. *Mater. Lett.*, 2004, **58**, 1183–1188.
59. Lima, M. D., Bonadimann, R., de Andrade, M. J., Toniolo, J. C. and Bergmann, C. P., Nnaocrystalline Cr_2O_3 and amorphous CrO_3 produced by solution combustion synthesis. *J. Eur. Ceram. Soc.*, 2006, **26**, 1213–1220.
60. Purohit, R. D., Saha, S. and Tyagi, A. K., Nanocrystalline ceria powders through citrate–nitrate combustion. *J. Nanosci. Nanotechnol.*, 2006, **6**, 209–214.
61. Chen, F., Sørensen, O. T., Meng, G. and Peng, D., Preparation of Nd-doped barium cerate through different routes. *Solid State Ionics*, 1997, **100**, 63–72.
62. Park, H.-B., Kweon, H.-J., Hong, Y.-S., Kim, S. J. and Kim, K., Preparation of $La_{1-x}Sr_xMnO_3$ powders by combustion of poly(ethylene glycol)–metal nitrate gel precursors. *J. Mater. Sci.*, 1997, **32**, 57–65.
63. Gostovic, D., Smith, J. R., Kundinger, D. P., Jones, K. S. and Wachsman, E. D., Three-dimensional reconstruction of porous LSCF cathodes. *Electrochem. Solid State Lett.*, 2007, **10**, B214–B217.